Published in final edited form as:
J Magn Reson Imaging. 2008 February ; 27(2): 356–367. doi:10.1002/jmri.21259.

MR-Guided Prostate Interventions

Clare Tempany, MD[*], **Sarah Straus**, **Nobuhiko Hata, PhD**, and **Steven Haker, PhD**
Department of Radiology, Brigham and Women's Hospital, and Harvard Medical School, Boston, Massachusetts

Abstract

In this article the current issues of diagnosis and detection of prostate cancer are reviewed. The limitations for current techniques are highlighted and some possible solutions with MR imaging and MR-guided biopsy approaches are reviewed. There are several different biopsy approaches under investigation. These include transperineal open magnet approaches to closed-bore 1.5T transrectal biopsies. The imaging, image processing, and tracking methods are also discussed. In the arena of therapy, MR guidance has been used in conjunction with radiation methods, either brachytherapy or external delivery. The principles of the radiation treatment, the toxicities, and use of images are outlined. The future role of imaging and image-guided interventions lie with providing a noninvasive surrogate for cancer surveillance or monitoring treatment response. The shift to minimally invasive focal therapies has already begun and will be very exciting when MR-guided focused ultrasound surgery reaches its full potential.

Keywords

prostate cancer; MR intervention; MR imaging; image registration; image segmentation

Prostate Cancer is a very common cancer and is a major public health issue in the world today. In the US, with an increase of the older age population as the "baby boomers" reach their 50s and beyond, the number of cases diagnosed per year is expected to more than double by the year 2015, when over 450,000 new cases of prostate cancer are expected to be diagnosed. This will place a significant burden on patients, their families, society, and healthcare. The disease-specific mortality from prostate cancer is low, with ≈4%–8% men dying of prostate cancer. While earlier diagnoses through more aggressive screening approaches is desirable, it is likely that many men with low tumor burden are being overtreated today.

Current trends in surgery are led by minimally invasive approaches and the use of image guidance. As they have rapidly gained popularity in medicine in general, the applications to the diagnosis and treatment of prostate cancer have similarly gained popularity. Many patients are seeking improved diagnostic methods and minimally invasive or even noninvasive image-guided treatment. In the future there will be increasing demands for less invasive diagnostic methods, monitoring, and surveillance techniques, as well as treatments with lower morbidity rates that will allow for control of the disease and minimize the treatment toxicities. This is supported not only by the growth in numbers of patients, but by the current limitations of diagnosis and therapy of prostate cancer.

*Address reprint requests to: C.T., Department of Radiology, Brigham & Women's Hospital, 75 Francis St., Boston, MA 02115. E-mail: E-mail: ctempany@bwh.harvard.edu.

Published online in Wiley InterScience (www.interscience.wiley.com).

Prostate cancer is currently diagnosed after the detection of an abnormal serum prostate-specific antigen (PSA) level and a prostate biopsy. It is most commonly asymptomatic and it is unusual for patients to present with clinical evidence of prostate cancer. In its advanced stages, prostate cancer can present with obstructive symptoms, such as difficulties in urination. The serum PSA is a blood test often done in men as they age, in some circumstances annually after age 50, and in certain high-risk men earlier, in their 40s. Much has been written about PSA, its measurement, and what the normalized values actually are. It is now clear that there are not only age-based normal ranges but also race-based ones (1,2). Although the routine use of PSA as a screening test is not accepted by all organizations, it is supported by the American Cancer Society (ACR) and the American Urological Association (AUA). Thus, it is now in widespread use and clearly provides very significant information for many men and their doctors today. The major source of serum PSA is from either benign prostatic hyperplasia (BPH) or prostate adenocarcinoma, with elevations above normal being due to one of the two diseases. Using various analyses, such as calculation of PSA density (accounting for total gland volume) it can be possible to predict if the PSA is due to cancer or BPH. As has been shown more recently by Efstathiou et al (3) the most useful application of PSA is as a serial assessment with the emphasis being on the rate of change or velocity of the PSA over time. It is also felt that it is important for men to establish a baseline PSA as early as 40 years of age and this be used to monitor any changes as the man ages. But in most men a biopsy is performed when the PSA is elevated above the expected normal range.

ULTRASOUND-GUIDED PROSTATE BIOPSY

Ultrasound (US) has widespread application and use in prostate imaging, being used both diagnostically and to provide image guidance for the transrectal US (TRUS) biopsy. US methods use gray scale imaging now occasionally supplemented by either color flow or Doppler imaging when available or as indicated. Prostate biopsies are done most often by using TRUS guidance to allow systematic sampling of the gland. However, despite advances in the imaging techniques and improved lesion detection and specificity with contrast agents, in the United States prostate US is almost exclusively a tool for biopsy guidance with gray scale methods and for placement of brachytherapy seeds during cancer treatments (Fig. 1). There are several different approaches to sampling the prostate gland during TRUS. Most initial biopsies will involve 6–12 cores removed with equal distributions from base to apex and right and left sides, supplemented with preferential lateral sampling. This is to ensure a widespread sampling directly to the peripheral zone, the site of origin of over 70% of prostate cancers. The procedure is usually performed in a urologist's office as an outpatient, typically taking less than 1 hour. The US probe is placed in the rectum, baseline images of the entire gland are obtained, and it is sampled with needles, 18-gauge biopsy guns, and equal numbers of cores taken from the right and left sides. It is rare for biopsies with US guidance to actually use image-based lesions for guiding sampling, most often it is used to visualize the gland and allow it to undergo systematic biopsies. The detection rate of prostate cancer with TRUS is 20%–40% in men with clinical suspicion of the disease. There are a significant number of false-negatives and many men who face repeated biopsies and rising PSA levels. Thus, many investigators are now working to improve the imaging tools for detection of focal abnormalities in the prostate that may be cancer. The most frequently investigated modality is magnetic resonance imaging (MRI), with research into many different MR parameters.

MRI OF THE PROSTATE

MR imaging of the prostate was first introduced in the late 1980s with large field-of-view, body coil methods at 1.5T (4). MR offered a major advance over the other modalities available, namely, computed tomography (CT) and US. For the first time it became possible to visualize the substructure of the prostate, with the peripheral and central zones reliably seen on T2-

weighted (T2W) images (Fig. 2). Focal areas of pathology were characterized and focal tumors in the peripheral zone were routinely represented by low signal lesions on T2W images. The central zone demonstrated the changes of benign prostate hyperplasia with mixed lesions of high signal (glandular epithelium) and low signal (stromal tissue) (Fig. 3). This ability led to applications of MRI for prostate cancer diagnosis, staging, and monitoring in drug trials (5–7).

CT is not routinely used for locoregional cancer staging, as it has poor contrast within the gland and cannot reliably determine the outer margins of the prostate, particularly at the base (near the bladder) and the apex, near the external urethral sphincter. Large lesions within the gland with advanced stages can be detected, especially early after intravenous (IV) contrast injection (Fig. 4). Smaller focal lesions cannot usually be seen within the gland. During therapy, however, CT does provide a reliable method for monitoring lymph node and bone metastases in advanced cases. CT of the abdomen and pelvis with both IV and oral contrast can detect retroperitoneal nodes. It cannot detect micrometastases (small deposits in a single node) within a node and relies on changes in nodal shape and size for depiction of metastatic nodes.

The most recent development in lymph node imaging is MRI lymphangiography. This method utilizes a contrast agent with ultrasmall iron oxide particles administered IV. The agent is taken up and fills normal lymph nodes and will not be taken up by nodes containing metastatic deposits. This provides a unique method for detection of small micrometastases within a normal-sized lymph node. This contrast agent is known as Fermuoxtran or Combidex, and is routinely used in Europe and has been assessed in clinical trials in the United States (8,9). The US Food and Drug Administration (FDA), however, has not approved the contrast agent for full clinical use.

Historical and Current MRI Protocols for Imaging and Staging Prostate Cancer

MRI of the prostate has evolved over the past two decades, starting in the late 1980s. The initial MRI of the prostate was performed using 1.5T MR magnets with the body coil for both transmitting and receiving the radiofrequency waves. The original protocols were composed of multiplanar T2W images supplemented with T1W images of the gland and retroperitoneum. As there were no surface coils suitable in the early days, all images were acquired with relatively large fields of view and thicker slices, thus limited in spatial resolution. This was the cornerstone of early prostate MRI work and was found to have value in depicting the normal anatomy of the prostate, its substructure, and the adjacent anatomy (7,10–12). Despite these limitations these methodologies led to increased application of prostate MRI in the clinic. These images were useful for locoregional staging and assessment of advanced diseases. These have been assessed in multiple studies as a tool for predicting the pathological stage of prostate cancer.

As the clinical demands changed to require higher spatial resolution and signal-to noise (SNR), in particular the demands for greater SNR, led to the introduction of endorectal coil (ecoil) (11,13). Thus, in the early 1990s most investigators began to evaluate the role of ecoil MRI in staging men with known prostate cancer (7). Multiple studies were conducted, including both single and multicenter prospective trials. One of the largest trials was conducted by the Radiology Diagnostic Oncology Group (RDOG) sponsored by the National Cancer Institute in the United States. This multicenter clinical trial enrolled men with biopsy-proven prostate cancer, scheduled, and selected to undergo radical prostatectomy. It consisted of two parts: the initial one, started in 1988, compared body coil MRI with US and the second in 1990 compared different ecoil imaging strategies (14). The results of the latter showed that MRI with ecoil was potentially a very useful examination in the staging evaluation of men with prostate cancer. The results, however, were variable and dependent on the expertise of the operator/radiologist interpreting the MR images. As the ecoil was a relatively new approach, this study was

performed somewhat early as a new technology. There was what appeared to be a "learning-curve" effect: with experience the radiologist got better and the results improved. Subsequent studies with decision support systems showed the learning effect (15,16). In the study by Seltzer et al (16) an overall improvement in receiver operator curves went from 0.60 to 0.80, with the addition of the computer analysis combined with the radiologist's interpretation. Getty et al (15) showed that there was a bigger improvement in staging accuracy when combined with PSA and Gleason score in the intermediate-risk patients. These latter are the patients most at need for help in staging as their clinical data and PSA are not definitive.

Since that time the MRI techniques continue to improve. One of the bigger advances was the introduction of fast spin echo (FSE) techniques, which markedly reduced the T2W sequences acquisition time, and when combined with the external phased array coils in combination with the ecoil allowed for major improvements in T2W image of the prostate.

Since these early studies, MRI has become a very popular and routinely used imaging study for men with prostate cancer. It has widespread applications ranging from cancer detection, staging, and treatment monitoring. There are now multiple different approaches to imaging the prostate with MRI and protocols are designed to answer specific questions such as tumor detection or staging a known cancer. There are many new "tissue enhancing" sequences being tested. At the same time the MRI technology (hardware and software) continues to evolve. The newer sequences currently being tested are proton spectroscopy (MRSI), dynamic contrast enhancement (DCE) (Fig. 5), and more recently diffusion imaging and ADC maps (17–23). Today many groups are testing these sequences either individually or as a multiparametric package of sequences.

OVERVIEW OF MR-GUIDED PROSTATE INTERVENTIONS

MR-guided prostate therapeutic interventions were introduced because MRI improved visualization of the prostate, its substructure, surrounding tissues, and, most important, focal lesions or cancer. There was an increasing demand for less invasive cancer treatments, which allowed for reduced morbidity and fewer side effects from conventional therapy such as radical prostatectomy and radiation therapy. The complications of radical prostatectomy are deep venous thrombosis, pulmonary embolism, urinary incontinence, and impotence. Radiation therapy has similar complications, with the addition of gastro-intestinal toxicity, such as rectal proctitis (24). The rationale of image-guided prostate intervention was thus to use the images to guide the delivery of treatment accurately, to maximize the treatment to the clinical target volume and minimize the treatment effects to any normal tissues nearby. Such new therapy options include cryotherapy (25), focused US therapy, as well as molecular therapies such as photodynamic therapy (26). For instance, image-guided cryotherapy of prostate has shown almost no risk of venous thrombosis and pulmonary embolism and a lower rate of urinary incontinence than radiation therapy (25). The development of the field of MR-guided interventions began with the introduction of the open configuration MRI device at the Brigham & Women's Hospital (Boston, MA) by Ferenc Jolesz (27), in collaboration with General Electric and investigators at the Brigham & Women's Hospital in 1993. This MRI unit, known as the Signa/Sp, was placed in an MRI-compatible operating room, operated at 0.5T field strength, and was originally designed for neurosurgical procedures. The device was the first of its kind, allowing for direct access to the patient in the bore of the magnet during open surgery such as craniotomy. The early applications of MR-guided interventions in neurosurgery and other clinical areas introduced unique and exciting novel approaches to complex clinical problems. The applications were extended to liver, kidney, breast, spine, and ear, nose, throat (ENT) pathologies. Given the open access afforded by the Signa SP, with its ability to allow lithotomy positioning, the prostate could be both imaged and accessed percutaneously using the transperineal approach.

MR-GUIDED PROSTATE CANCER BRACHYTHERAPY

The clinical efficacy of MRI to guide prostate brachytherapy has been demonstrated by Drs. D'Amico and Tempany et al (28). The initial report in 1998 (29) described the experience in nine patients who underwent transperineal MRI-guided prostate brachytherapy in the Signa/SP open-configuration 0.5T MRI scanner. The interventional device comprised an MRI-compatible perineal template and a rectal obturator that was inserted through the template for rectal access. A real-time intraoperative MRI sequence was obtained throughout the prostate gland, on which the dosimetry plan was performed in the procedure room. The patient was positioned in the lithotomy position and the procedure performed under general anesthesia. The radiologist, based on the axial T2W image, defined the clinical target volume, or the peripheral zone. The peripheral zone (PZ) of the prostate gland, anterior rectal wall, and prostatic urethra, as defined by MR images, were identified and contoured in a surgical simulation and navigation tool, the 3D Slicer (30), with resultant volumes calculated. These data were then transferred to the radiation treatment planning software program (31) this allows the medical physicist and radiation oncologist to review all images, all volumes, and plan the optimal seed distribution throughout the gland (Fig. 6). Multiple needles were then preloaded with I-125 sources and placed in the gland under real-time image guidance by fast gradient echo (FGR) imaging. Each needle placed was imaged and assessed for location by imaging and repositioned if necessary—if not it was then assessed by the medical physicist for dosimetric accuracy and if appropriate the seeds were dropped. This iterative process continued for all planned needles. As the implant progressed it would be apparent if new or extra needles/seeds would be required. After consultation these were added and then final dosimetry was assessed in all cases. The patient was admitted for overnight stay in the hospital and following successful removal of the urinary catheter the next day was discharged. All men returned for follow-up imaging at 6 weeks with both MR and CT examinations obtained to allow for final dosimetry calculations.

The implant procedure achieved a successful radiation dose of 160 Gy in 89%–99% (median 94%) of the clinical target volume, while 42%–89% (median 70%) of the volume of the anterior rectal wall received doses that were below the tolerance.

A different approach was taken by Susil et al (33) and Menard et al (32), who reported the use of a 1.5T closed-bore scanner for transperineal MR-guided brachytherapy. High-dose radiation therapy with Iridium-192 sources was used for brachytherapy. Patients were situated in the left lateral decubitus position to maximize perineal exposure in the 1.5T MRI Scanner bore (Siemens Sonata, Siemens Medical Systems, Erlangen, Germany). The radiation was delivered to the prostate via hollow closed-tip catheters, which were inserted through the perineum and into the prostate gland. They developed a customized needle guiding template attached to a positioning arm (Siemens Medical Systems) for orienting needles according to the treatment plan. Following the acquisition of three plane scout images and a 3D steady state free precession (SSFP) sequence of the template, pubic arch, and prostate gland, fast spin echo axial images were taken for targeting and verification of catheter positions. An endorectal imaging coil (USA Instruments, Aurora, OH) on the needle guiding device allowed for high-quality prostate MRI for planning and needle guidance. Once the catheters had been inserted outside the scanner the patient was reimaged with FSE images which confirmed needle-placement and axial, coronal, and sagittal T2W FSE images were acquired for dosimetry planning. After successful catheter placement, patients were transferred to an oncology treatment room and high-dose radiation was delivered.

In a report of 10 procedures on five patients (32), the median percentage of volume receiving 100% of prescribed minimal peripheral dose (V(100)) achieved was 94% (mean, 92%; 95%

confidence interval, 89%–95%). The urethral V (125) ranged from 0%–18% (median, 5%), and the rectal V (75) ranged from 0%–3.1% (median, 0.3%).

Albert et al (34) later reported that rectal bleeding after MRI-guided prostate brachytherapy monotherapy was infrequent and urethral and bladder toxicity was rare, presumably due to the ability to perform a careful urethral-sparing technique with the MRI-guided approach. Subsequent reports from the same team indicated that MRI-guided brachytherapy is a safe alternative to US-guided brachytherapy (35–39).

These two approaches to MRI guidance in prostate cancer treatment have been very successfully applied and demonstrate an added advantage of including MRI at all steps in the process, from initial staging through treatment and for posttreatment follow-up. Newer approaches include using MRI/MRSI in guiding intensity modulated radiation treatments (IMRT) and will likely lead to an improved ability to deliver higher does to the actual tumor, while sparing more and more normal tissues. This is expected to lower the toxicity profiles and improve patient outcomes. Thus, future opportunities will be dependent on improved MRI and cancer definition.

MR-GUIDED BIOPSY

The introduction of MRI-guided transperineal prostate biopsy was originally made possible by extending the system and methods used in MRI-guided brachytherapy in the Signa/sp open-configuration MRI scanner (40–42). It was clear that with the increasing abilities of MR images to detect focal tumors an MRI-guided biopsy method became essential to allow direct sampling of these focal lesions. The group at Brigham and Women's Hospital introduced an MRI-guided prostate biopsy program in the Signa/Sp system which uses the transperineal approach with direct real-time image-guided sampling of the prostate and any suspicious lesions.

There is a significant clinical need, with many men having negative biopsy results and rising PSA levels. In a prospective MR-guided prostate biopsy study our patients were selected for the procedure when they were suspected of having prostate cancer due to elevation of the PSA level and had had several negative TRUS biopsies, or were unable to have TRUS biopsies as they had prior rectal surgery. All men meeting these eligibility criteria were enrolled and had prebiopsy imaging at 1.5T with ecoil, with multiparametric MRI exams. These included T2W, T1W images, and gadolinium and MRSI sequences.

After assessment by anesthesia and preadmission testing the patients came to the MRT suite for the procedure. Patients were placed in the lithotomy position and the procedure was done under general anesthesia (Fig. 7). The patients were reimaged with T1 and T2W sequences and with all images available the radiologist defined all suspicious lesions or targets within the prostate. These were selected for biopsy, as well as either sextant or octant sampling regimes, as is done conventionally. After all prospective sample locations were defined by the radiologist the coordinates were transferred to the 3D Slicer to allow for registration to the images and display of the targets during needle insertion. The needles were guided by fast gradient-recalled echo and T2W FSE images (Fig. 7). Surgical navigation software (3D Slicer, www.slicer.org) was adapted to assist in targeting the peripheral zone and tumor (42). 3D Slicer effectively enables direct T2W visualization of the peripheral zone of the prostate with the real-time image containing the biopsy needle and visualized in the same frame of reference. Simulations such as these are made possible by resampling the preloaded 0.5T axial and sagittal T2W FSE images just minutes prior to needle placement (42). The 3D Slicer is also applied to postprocessing of intraoperative MRI from prostate therapies. Other features of the 3D Slicer include automated registration, segmentation, and an interface for manual contouring within images (Fig. 8).

The sextant and targeted biopsy of suspected lesions was performed with a perineal template and an MRI-compatible single action biopsy needle (Single Action Biopsy Device; U.S. Biopsy, Franklin, IN, or MRI BIO-GUN Automated Biopsy System, EZ-EM, Lake Success, NY). The 18-gauge needles had a 20 mm throw and trocar tip. For each needle placement a hole for guiding the biopsy needle toward the target was selected and the physician was notified about target depth. Each biopsy specimen/core was carefully labeled according to the location it came from, prior to submission to the Department of Pathology. This allowed for site-specific pathology to be obtained and ultimately for image/lesion pathological correlation. The program has successfully performed over 50 biopsy cases to date with results of 30% positive sampling rates (43). After the successful implementation of MRI-guided biopsy in an open-configuration scanner, other teams reported MRI-guided biopsy procedures in higher field closed-bore MR magnets.

The joint team from Johns Hopkins University and the National Institutes of Health demonstrated the use of a closed-bore scanner system that enabled precise guidance and monitoring of transrectal prostate interventions with a 1.5T MRI unit. The primary challenge of creating a closed-bore interventional device was the development of a mechanical needle guide that could safely and accurately guide the treatment needle to the lesion while the patient remained inside the closed-bore scanner. The team overcame this challenge by developing a remotely operated needle guide, an ecoil, and an associated planning and imaging control method. They designed a customized rectal sheath and needle guide with a remotely operated endorectal transceiver coil and tracking coils for imaging (Fig. 9). A canine study indicated that the newly developed system can target lesions under real-time fast GRE with accuracy less than 2 mm (44). The clinical application of the transrectal device was MR-guided intraprostatic placement of gold fiducial markers (four procedures) and/or prostate biopsy (three procedures) to the patient scheduled to receive a standard course of conformal external beam radiation therapy. The procedures were performed under local anesthesia for on average 76 minutes (maximum 93 minutes, minimum 60 minutes). Needle placement was confirmed using regular T1-weighted fast spin-echo sequence taking 1 minute, 20 seconds for scanning (45,46).

The same team from Johns Hopkins University and the National Institutes of Health also performed transperineal biopsy procedures (33). All procedures were again performed under local anesthesia. After registration of the perineal grid, biopsy sites were selected, a grid hole and insertion depth for each site were read from the targeting application, the patient table was withdrawn from the scanner, and MR-compatible 14-gauge beveled biopsy needles were inserted (MRI Devices, Waukesha, WI). The patient was then advanced back into the scanner and, prior to tissue collection, FSE images were acquired to verify placement of the needles.

In another study (47), transrectal prostate biopsy was performed with the patient positioned prone in a 1.5T closed-bored MRI unit (Magnetom Vision or Magnetom Sonata; Siemens). Five patients underwent MRI-guided biopsy immediately after diagnostic MRI, and seven patients underwent MRI-guided biopsy in a second session within 2 weeks after the initial MR examination. They also developed a customized MRI-compatible device to guide the needle to a predefined location in the prostate gland. The device consisted of a base plate, an adjustable arm, and a needle guide filled with contrast material gel that could be visualized at MR imaging.

After the patient was positioned the needle guide was inserted into the rectum and connected to the arm of the biopsy device. The arm enables the needle guide to be rotated, moved forward and backward, and adjusted in height. In addition, the insertion angle can be changed by rotating the needle guide about a point inside the rectum. The needle guide can be rotated and moved forward and backward from outside the MR unit by means of a telescopic rod. It is thus possible to direct the needle guide to the desired prostate region with MRI guidance (47). An oblique

transverse T2W turbo SE sequence was performed before biopsy. The biopsy device was positioned with imaging guidance by using a half-Fourier rapid acquisition with relaxation enhancement (RARE) sequence. The sampling was combined targeted and octant biopsy. The general scheme of systematic octant biopsy was used for orientation, while two samples were taken at a tumor foci and only one sample was taken from regular nonsuspicious octant sites. With this approach, Beyersdorff et al (47) sampled a total of 40 sites in 12 patients as suspicious areas, and the other 56 sites were sampled as part of octant biopsy.

The last clinical report available as of preparation of this article was a study conducted by Engelhard et al (48), in which transrectal biopsy was performed using a closed-bore 1.5T scanner. Thirty-seven consecutive men were included. They used the same method as described above with a needle guide manually fed under MRI control to the location to be punctured close by the prostate capsule and the direction of the puncture was defined (48). The biopsy procedure was performed with the patient in the supine position. Prebiopsy imaging using an ecoil was performed immediately before the biopsy procedure to identify the suspicious lesion. After the prebiopsy imaging, the ecoil was removed and the biopsy device was inserted into the patient's rectum. Needle placement was observed using a TrueFisp sequence and a TSE sequence was used for confirmation of successful placement of the needle tip in the lesion.

The motivation for using interventional devices is clear: mechanical placement can control the needle more accurately than manual placement and facilitates access to the patient in the closed-form scanner. Thus, research institutions are developing mechanical devices to align needles and other surgical instruments under MRI-guidance. The application of a commercial MRI-compatible robot in prostate interventions is on the horizon; Zangos et al (49) reported the first cadaveric study results using a commercial MR-guided assistance system, Innomotion (Innomedic, Herxheim, Germany), for transgluteal needle placement in the prostate gland. As higher-tesla close-bore magnets become available for MRI, the strong magnetic field prevents the use of conventional mechatronics and the confined physical space makes it extremely challenging to access the patient. Fischer et al have designed a robotic assistant system that overcomes these difficulties and promises safe and reliable intra-prostatic needle placement inside closed 3T MRI scanners (81). The robot operates in the space between the patient's legs without interference with the patient, MRI scanner components, anesthesia equipment, and auxiliary equipment present as shown in Figure 8.

In conclusion, MR-guided biopsy and brachytherapy has proven to be a useful alternative or second approach to US-guided procedures due to the high sensitivity of MRI for detecting prostate tumors, high spatial resolution, excellent soft-tissue contrast, and multiplanar volumetric imaging capabilities. Further development of image registration, display, and needle placement devices will be indispensable for the advancement of more clinical studies.

PROSTATE MR IMAGE REGISTRATION

Image registration is the process whereby different images or image volumes, possibly taken at different times and using different devices, are brought into anatomical alignment. The fundamental purpose of registration is to increase the information content of images used by the physician during therapy by providing unified views of all preoperative MRI with intraoperative imaging. In this way therapy can be targeted specifically to those locations where it is likely to be most effective. Registration methods can be applied to MR-guided therapy, but are applicable to procedures guided by US and CT as well. Thus, MRI may help give procedural guidance even when the principal imaging modality used during therapy is not MR. This undoubtedly increases the potential for the use of MR for therapy guidance.

Prostate image registration is difficult because the prostate consists of soft tissue and can deform, depending on the circumstances surrounding the procedure. It is important to recognize

that the prostate gland can move considerably during procedures. Prostate location can be affected by patient position, leg position, and the presence of an ecoil. Hirose et al (50) conducted a study to evaluate the effect of changes in leg position and the presence or absence of an ecoil on prostate shape and location. They showed that significant changes in prostate shape and position relative to surrounding anatomy could occur due to changes in leg position and the use of an ecoil. In Kim et al (51) the authors conducted a study on expandable and rigid ecoils used for prostate imaging. They showed that an expandable coil rigid registration was more difficult, relative to the use of a rigid coil, due to a greater change in prostate shape. Steenbakker et al's (52) approach was to evaluate the effect of knee support and shape of the tabletop on rectum and prostate position. They concluded that the rectum and prostate were significantly shifted dorsally by the use of a knee support, while the shape of the tabletop did not influence the rectum or prostate position. Nichol et al (53) used a finite element technique to determine the degree of prostate deformation due to radiotherapy, transurethral resection of the prostate (TURP), and bladder and bowel filling.

Registration Methodology

Image registration in general, and when applied to the prostate, can be roughly categorized according to the method used to assess the quality of image alignment, the type of transformations that are considered for alignment, and the necessity of landmarks or contours or image segmentation to guide the registration. The number of approaches to image registration is vast, and there is currently a great deal of ongoing work in the area. We briefly review some of the more popular methods, as applied to the prostate.

Finite Element Methods—This method models tissues in a way that accounts for their materiel properties, such as their compressibility and deformation under stress. In this way these registration transformations are more general and potentially more realistic than rigid ones. In Bharatha et al (54) the authors aligned pretreatment 1.5T magnetic resonance images, taken with an ecoil, with 0.5T intraoperative images taken without an ecoil. The results showed that the method significantly improved the quality of match as compared to rigid registration (Fig. 10). In Alterovitz et al (55) the authors registered diagnostic probe-in MR images to therapeutic probe-out MR images for treatment planning, modeling the prostate, as well as surrounding tissue. The method allowed for estimation of the parameters that characterize tissue structures.

Thin-Plate Spline Registration—Thin-plate spline methods of registration are popular because they are fast and more general than rigid registration. These methods are based on the direct registration of corresponding landmark points in two image datasets. These landmark points may be determined either manually or by an automated process. The thin-plate spline is essentially an interpolation method; it yields a parametric form of a registration transformation function that sends the landmarks in one image to the corresponding landmarks in the other, and at the same time smoothly interpolates this formula to all of the other points in the image. Other authors (56,57) conducted studies on the ability to improve registration results as compared to rigid registration by using a nearly automated combination of thin-plate splines and a mutual information measure of image agreement. Similarly, in Venugopal et al (58) the authors conducted a feasibility study on the use of thin-plate splines to allow the use of MR spectroscopy during prostate cancer therapy.

Mutual Information-Based Methods—Nearly all image registration algorithms can be described as the optimization of a function that measures agreement between images. Mutual information (MI) methods attempt to align images by maximizing an information-theoretic measure of the degree to which the information content of one image set is contained in or is explained by the information content of the other. It is a particularly popular method to use

when aligning imaging from different modalities, such as MR and US, or MR and CT. It can also be used to align imaging obtained using differing MR parameters, such as T1 and T2 weighting. Effective use of a 3D MI registration method to register MR volumes of the pelvis and prostate for MR-guided prostate treatment has been reported (59,60). In another study (61), MI was used in the registration of MR spectroscopy, having the potential to be used in treatment planning. In Lee et al (62) the authors report on a technique for MI-based automatic registration of MR and SPECT prostate images.

Segmentation Based on Deformable Models—Some methods of registration require a segmentation of one or more of the image datasets being registered. Segmentation is a process whereby individual structures within images are identified. Segmentation can be done manually or using algorithmic automation. To date, there has been only limited research on automatic segmentation of prostate MRI. The authors in Pasquier et al (63) used a 3D computer model of the prostate gland, deforming it so it agreed with T2W and T1W image information. Statistical tests were performed to demonstrate robustness and agreement to ground truth obtained by manual segmentation. An automated segmentation algorithm using a model of prostate shape and variation was reported (64). The method allowed for the simultaneous identification of other relevant anatomic structures, such as the rectum and internal obturator muscles, through the creation of a multistructure model. Information-theoretic measures were used to guide the segmentation.

Applications of Prostate MR Image Registration

One of the great potential benefits of image registration is its ability to incorporate all patient imaging into a single multimodality dataset. This allows for the utilization of imaging that may not be available during therapy due to time constraints or the choice of imaging modality that is used during therapy. In Barnes et al (65) the authors used MR spectroscopy, obtained prior to biopsy, to guide the placement of a needle during MR-guided biopsy. Image registration was used to find the target location within intraoperative imaging. Image fusion also allows for the joint analysis of multiple image types. In Chan et al (66) the authors used line-scan diffusion, T2-mapping, and T2W imaging in combination with a machine-learning classifier to determine image locations most likely to contain cancer. In work by another group, fusion of 1.5T MR imaging with color-Doppler US was performed and showed that in combination the accuracy of pathological staging could be improved. Ground truth was obtained by pathological examination following prostatectomy (67).

One simple application of registration of prostate images for therapy is to improve the estimation and delineation of the glandular capsule. The use of TRUS versus MRI in the estimation of the prostate volume was compared (68). In that study, a comparison of the prostate volumes measured with MRI and TRUS was made with surgical specimen volumes. The authors concluded that MRI is more accurate than TRUS for determining the prostate volume, but suggested that for reasons of cost, TRUS is typically preferred. In Rahmouni et al (69) the authors assessed the accuracy of in vivo measures of prostatic volume by MRI and ultrasonography, using the wet weight of the excised specimen as ground truth, and concluded that contoured MRI was superior to linear MRI or TRUS in estimating prostate volume. Analysis of segmentation using TRUS, CT, and MR was performed in Smith et al (70) and showed that there are systematic differences in the variability of segmentation. Not surprisingly, MR and TRUS had the smallest variability and closest correspondence.

Registration of MR and MR Spectroscopy to CT—As CT is so commonly used for radiation planning and guidance it would be useful to integrate MR into these planning systems. Schreibmann and Xing (71) used a registration method in initial clinical tests to register preoperative MRI and MR spectroscopic imaging to CT imaging used for radiation therapy

planning. This promising method used normalized correlation as the measure of image agreement and incorporated a "narrow band" method to limit the registration to relevant structures. Normalized correlation is similar to MI in that it is appropriate for differing modalities, where direct comparison of image intensities is inappropriate. A nonrigid registration method for aligning preoperative MR spectroscopy, US, and CT for treatment planning has been described (72). It is based on the alignment of contours delineating the prostate gland in axial imaging. The method is able to account for deformation due to the use of an ecoil.

MR-Guided TRUS for Prostate Biopsy—US is commonly used for guiding prostate biopsies. This would be of major value if we had algorithms to allow accurate registration of MR to US during a biopsy. Initial work has been shown in Lattouf et al (73) and the authors reported on MRI-imaging-directed TRUS-guided biopsies. They sought to test whether using ecoil MRI during TRUS-guided biopsies increases the yield. They found higher cancer yields, but the difference was not statistically significant. They suggested that better localization of targets within the MRI and accurate registration methods might improve the result. This work is now being pursued by several groups, including ours, to allow for accurate real-time registration of preprocedure MRI to TRUS images.

MR-Guided TRUS for Prostate Brachytherapy—Promising initial work has been done on the use of MRI during TRUS-guided brachytherapy (Fig. 11). Authors (74,75) have shown that fusing preoperative MR to intraoperative US can help to prevent underestimation of prostate volume, especially at the apex and base, with a positive impact on treatment planning.

NEW PROSTATE CANCER TREATMENTS: FOCAL THERAPY

Most current treatments for low-risk localized prostate cancer are global in that they aim to treat the entire prostate gland, as if it was filled equally with prostate cancer. This approach has been successful; it may in fact be overly aggressive. There are significant side effects to all global treatments. The low likelihood of mortality leads many to question the possibilities of focal therapy. The other clinical population currently under-served are men who are presenting for salvage therapies after radiation has failed or have bulky disease and may benefit from a focal ablation such as MR-guided focused US (MRgFUS) surgery prior to radiation. This is a major paradigm shift which is not universally accepted at this time. However, with major improvements in focal ablation techniques this approach becomes very compelling.

MRgFUS is a novel and unique approach to thermal ablation. It involves MRI to define, guide, monitor, and control the energy delivery to a target organ or lesion. It has been in use under US guidance as high-intensity focused US (HIFUS) for many years. In the prostate, Gelet et al (76) were the first to evaluate and publish the results of HIFUS transrectal 2.25 MHz device (Ablatherm) in 14 patients with localized prostate cancer. Early results are very promising (77). MR guidance offers the unique ability to obtain direct real-time thermometry during the ablation or surgical procedure (78). The group at Brigham and Women's Hospital has shown its value in treatment of diseases of the breast (79) and uterus (80). Currently, research is being carried out to test the use of MR-guided HIFUS for treatment of prostate cancer.

CONCLUSION

MRI and its unique monitoring and guidance capability has so much to offer in the diagnosis and therapy of prostate cancer. This disease has such a major impact on patients, their families, and all aspects of the health-care systems worldwide that it is critical that research and clinical applications of image-guided therapy continue and become a more widespread reality for all men.

Acknowledgements

The authors thank Angela Kanan-Roddy, Daniel Kacher, Janice Fairhurst, Robert Cormack, Anthony D'Amico, Axel Krieger, Minna So, and Jerome Richie for assistance and support.

Contract grant sponsor: National Institutes of Health (NIH); Contract grant numbers: AG 19513, CA 104976, CA 109246, RR 19703, CA067165, EB005149, and CA111288.

References

1. Gray MA, Delahunt B, Fowles JR, Weinstein P, Cookes RR, Nacey JN. Demographic and clinical factors as determinants of serum levels of prostate specific antigen and its derivatives. Anticancer Res 2004;24:2069–2072. [PubMed: 15274402]
2. Powell IJ, Banerjee M, Novallo M, et al. Should the age specific prostate specific antigen cutoff for prostate biopsy be higher for black than for white men older than 50 years? J Urol 2000;163:146, 148. [PubMed: 10604333]discussion 148–149
3. Efstathiou JA, Chen MH, Catalona WJ, et al. Prostate-specific antigen-based serial screening may decrease prostate cancer-specific mortality. Urology 2006;68:342–347. [PubMed: 16904449]
4. Cheng D, Tempany CM. MR imaging of the prostate and bladder. Semin Ultrasound CT MR 1998;19:67–89. [PubMed: 9503521]
5. Ellis JH, Tempany C, Sarin MS, Gatsonis C, Rifkin MD, McNeil BJ. MR imaging and sonography of early prostatic cancer: pathologic and imaging features that influence identification and diagnosis. AJR Am J Roentgenol 1994;162:865–872. [PubMed: 8141009]
6. Tempany CM, Partin AW, Zerhouni EA, Zinreich SJ, Walsh PC. The influence of finasteride on the volume of the peripheral and periurethral zones of the prostate in men with benign prostatic hyperplasia. Prostate 1993;22:39–42. [PubMed: 7678931]
7. Tempany CM, Rahmouni AD, Epstein JI, Walsh PC, Zerhouni EA. Invasion of the neurovascular bundle by prostate cancer: evaluation with MR imaging. Radiology 1991;181:107–112. [PubMed: 1887017]
8. Harisinghani MG, Barentsz J, Hahn PF, et al. Noninvasive detection of clinically occult lymph-node metastases in prostate cancer. N Engl J Med 2003;348:2491–2499. [PubMed: 12815134]
9. Harisinghani MG, Saini S, Weissleder R, et al. MR lymphangiography using ultrasmall superparamagnetic iron oxide in patients with primary abdominal and pelvic malignancies: radiographic-pathologic correlation. AJR Am J Roentgenol 1999;172:1347–1351. [PubMed: 10227514]
10. Schnall MD, Imai Y, Tomaszewski J, Pollack HM, Lenkinski RE, Kressel HY. Prostate cancer: local staging with endorectal surface coil MR imaging. Radiology 1991;178:797–802. [PubMed: 1994421]
11. Schnall MD, Lenkinski RE, Pollack HM, Imai Y, Kressel HY. Prostate: MR imaging with an endorectal surface coil. Radiology 1989;172:570–574. [PubMed: 2748842]
12. Way WG Jr, Brown JJ, Lee JK, Gutierrez E, Andriole GL. MR imaging of benign prostatic hypertrophy using a Helmholtz-type surface coil. Magn Reson Imaging 1992;10:341–349. [PubMed: 1383669]
13. Schnall MD, Bezzi M, Pollack HM, Kressel HY. Magnetic resonance imaging of the prostate. Magn Reson Q 1990;6:1–16. [PubMed: 1696493]
14. Tempany CM, Zhou X, Zerhouni EA, et al. Staging of prostate cancer: results of Radiology Diagnostic Oncology Group project comparison of three MR imaging techniques. Radiology 1994;192:47–54. [PubMed: 8208963]
15. Getty DJ, Seltzer SE, Tempany CM, Pickett RM, Swets JA, McNeil BJ. Prostate cancer: relative effects of demographic, clinical, histologic, and MR imaging variables on the accuracy of staging. Radiology 1997;204:471–479. [PubMed: 9240538]
16. Seltzer SE, Getty DJ, Tempany CM, et al. Staging prostate cancer with MR imaging: a combined radiologist-computer system. Radiology 1997;202:219–226. [PubMed: 8988214]
17. desouza NM, Reinsberg SA, Scurr ED, Brewster JM, Payne GS. Magnetic resonance imaging in prostate cancer: the value of apparent diffusion coefficients for identifying malignant nodules. Br J Radiol 2007;80:90–95. [PubMed: 17303616]

18. Futterer JJ, Heijmink SW, Scheenen TW, et al. Prostate cancer localization with dynamic contrast-enhanced MR imaging and proton MR spectroscopic imaging. Radiology 2006;241:449–458. [PubMed: 16966484]
19. Gibbs P, Tozer DJ, Liney GP, Turnbull LW. Comparison of quantitative T2 mapping and diffusion-weighted imaging in the normal and pathologic prostate. Magn Reson Med 2001;46:1054–1058. [PubMed: 11746568]
20. Kozlowski P, Chang SD, Jones EC, Berean KW, Chen H, Golden-berg SL. Combined diffusion-weighted and dynamic contrast-enhanced MRI for prostate cancer diagnosis—correlation with biopsy and histopathology. J Magn Reson Imaging 2006;24:108–113. [PubMed: 16767709]
21. Mulkern RV, Barnes AS, Haker SJ, et al. Biexponential characterization of prostate tissue water diffusion decay curves over an extended b-factor range. Magn Reson Imaging 2006;24:563–568. [PubMed: 16735177]
22. Scheenen TW, Klomp DW, Roll SA, Futterer JJ, Barentsz JO, Heerschap A. Fast acquisition-weighted three-dimensional proton MR spectroscopic imaging of the human prostate. Magn Reson Med 2004;52:80–88. [PubMed: 15236370]
23. Yu KK, Scheidler J, Hricak H, et al. Prostate cancer: prediction of extracapsular extension with endorectal MR imaging and three-dimensional proton MR spectroscopic imaging. Radiology 1999;213:481–488. [PubMed: 10551230]
24. Salomon L, Levrel O, Anastasiadis AG, et al. Outcome and complications of radical prostatectomy in patients with PSA <10 ng/ml: comparison between the retropubic, perineal and laparoscopic approach. Prostate Cancer Prostatic Dis 2002;5:285–290. [PubMed: 12627213]
25. Bahn DK, Lee F. Cryosurgical ablation therapy for prostate cancer. Arch Ital Urol Androl 2000;72:302–304. [PubMed: 11221060]
26. Weersink RA, Bogaards A, Gertner M, et al. Techniques for delivery and monitoring of TOOKAD (WST09)-mediated photodynamic therapy of the prostate: clinical experience and practicalities. J Photochem Photobiol 2005;79:211–222.
27. Schenck JF, Jolesz FA, Roemer PB, et al. Superconducting open-configuration MR imaging system for image-guided therapy. Radiology 1995;195:805–814. [PubMed: 7754014]
28. D'Amico AV, Tempany CM, Schultz D, et al. Comparing PSA outcome after radical prostatectomy or magnetic resonance imaging-guided partial prostatic irradiation in select patients with clinically localized adenocarcinoma of the prostate. Urology 2003;62:1063–1067. [PubMed: 14665356]
29. D'Amico AV, Cormack R, Tempany CM, et al. Real-time magnetic resonance image-guided interstitial brachytherapy in the treatment of select patients with clinically localized prostate cancer. Int J Radiat Oncol Biol Phys 1998;42:507–515. [PubMed: 9806508]
30. Gering DT, Nabavi A, Kikinis R, et al. An integrated visualization system for surgical planning and guidance using image fusion and an open MR. J Magn Reson Imaging 2001;13:967–975. [PubMed: 11382961]
31. Cormack, RA.; D'Amico, AV.; Kooy, HM.; Tempany, CM. Brigham and Women's Hospital, assignee. Radiation seed implant method and apparatus. USA patent 6311084. Oct 30. 2001
32. Menard C, Susil RC, Choyke P, et al. MR guided HDR prostate brachytherapy in standard 1.5T scanner. Int J Radiat Oncol Biol Phys 2004;59:1414–1423. [PubMed: 15275727]
33. Susil RC, Camphausen K, Choyke P, et al. System for prostate brachytherapy and biopsy in a standard 1.5 T MRI scanner. Magn Reson Med 2004;52:683–687. [PubMed: 15334592]
34. Albert M, Tempany CM, Schultz D, et al. Late genitourinary and gastrointestinal toxicity after magnetic resonance image-guided prostate brachytherapy with or without neoadjuvant external beam radiation therapy. Cancer 2003;98:949–954. [PubMed: 12942561]
35. Cormack RA, Kooy H, Tempany CM, D'Amico AV. A clinical method for real-time dosimetric guidance of transperineal 125I prostate implants using interventional magnetic resonance imaging. Int J Radiat Oncol Biol Phys 2000;46:207–214. [PubMed: 10656394]
36. D'Amico A, Cormack R, Kumar S, Tempany CM. Real-time magnetic resonance imaging-guided brachytherapy in the treatment of selected patients with clinically localized prostate cancer. J Endourol 2000;14:367–370. [PubMed: 10910153]
37. D'Amico AV, Cormack RA, Tempany CM. MRI-guided diagnosis and treatment of prostate cancer. N Engl J Med 2001;344:776–777. [PubMed: 11236795]

38. Das P, Chen MH, Valentine K, et al. Using the magnitude of PSA bounce after MRI-guided prostate brachytherapy to distinguish recurrence, benign precipitating factors, and idiopathic bounce. Int J Radiat Oncol Biol Phys 2002;54:698–702. [PubMed: 12377320]
39. Hurwitz MD, Cormack R, Tempany CM, Kumar S, D'Amico AV. Three-dimensional real-time magnetic resonance-guided interstitial prostate brachytherapy optimizes radiation dose distribution resulting in a favorable acute side effect profile in patients with clinically localized prostate cancer. Tech Urol 2000;6:89–94. [PubMed: 10798806]
40. Cormack RA, D'Amico AV, Hata N, Silverman S, Weinstein M, Tempany CM. Feasibility of transperineal prostate biopsy under interventional magnetic resonance guidance. Urology 2000;56:663–664. [PubMed: 11018628]
41. D'Amico AV, Tempany CM, Cormack R, et al. Transperineal magnetic resonance image guided prostate biopsy. J Urol 2000;164:385–387. [PubMed: 10893591]
42. Hata N, Jinzaki M, Kacher D, et al. MR imaging-guided prostate biopsy with surgical navigation software: device validation and feasibility. Radiology 2001;220:263–268. [PubMed: 11426008]
43. So, MJ.; Haker, S.; Zou, KH., et al. Clinical evaluation of MR-guided prostate biopsy. Proc ISMRM; Miami. 2005. p. 264
44. Susil RC, Krieger A, Derbyshire JA, et al. System for MR image-guided prostate interventions: canine study. Radiology 2003;228:886–894. [PubMed: 12954903]
45. Krieger A, Susil RC, Menard C, et al. Design of a novel MRI compatible manipulator for image guided prostate interventions. IEEE Trans Biomed Eng 2005;52:306–313. [PubMed: 15709668]
46. Susil RC, Menard C, Krieger A, et al. Transrectal prostate biopsy and fiducial marker placement in a standard 1.5T magnetic resonance imaging scanner. J Urol 2006;175:113–120. [PubMed: 16406885]
47. Beyersdorff D, Winkel A, Hamm B, Lenk S, Loening SA, Taupitz M. MR imaging-guided prostate biopsy with a closed MR unit at 1.5 T: initial results. Radiology 2005;234:576–581. [PubMed: 15616117]
48. Engelhard K, Hollenbach HP, Kiefer B, Winkel A, Goeb K, Engehausen D. Prostate biopsy in the supine position in a standard 1.5-T scanner under real time MR-imaging control using a MR-compatible endorectal biopsy device. Eur Radiol 2006;16:1237–1243. [PubMed: 16447048]
49. Zangos S, Herzog C, Eichler K, et al. MR-compatible assistance system for punction in a high-field system: device and feasibility of transgluteal biopsies of the prostate gland. Eur Radiol 2007;17:1118–1124. [PubMed: 17031454]
50. Hirose M, Bharatha A, Hata N, et al. Quantitative MR imaging assessment of prostate gland deformation before and during MR imaging-guided brachytherapy. Acad Radiol 2002;9:906–912. [PubMed: 12186439]
51. Kim Y, Hsu IC, Pouliot J, Noworolski SM, Vigneron DB, Kurhanewicz J. Expandable and rigid endorectal coils for prostate MRI: impact on prostate distortion and rigid image registration. Med Phys 2005;32:3569–3578. [PubMed: 16475755]
52. Steenbakkers RJ, Duppen JC, Betgen A, et al. Impact of knee support and shape of tabletop on rectum and prostate position. Int J Radiat Oncol Biol Phys 2004;60:1364–1372. [PubMed: 15590166]
53. Nichol AM, Brock KK, Lockwood GA, et al. A magnetic resonance imaging study of prostate deformation relative to implanted gold fiducial markers. Int J Radiat Oncol Biol Phys 2007;67:48–56. [PubMed: 17084546]
54. Bharatha A, Hirose M, Hata N, et al. Evaluation of three-dimensional finite element-based deformable registration of pre- and intraoperative prostate imaging. Med Phys 2001;28:2551–2560. [PubMed: 11797960]
55. Alterovitz R, Goldberg K, Pouliot J, et al. Registration of MR prostate images with biomechanical modeling and nonlinear parameter estimation. Med Phys 2006;33:446–454. [PubMed: 16532952]
56. Fei B, Duerk JL, Sodee DB, Wilson DL. Semiautomatic nonrigid registration for the prostate and pelvic MR volumes. Acad Radiol 2005;12:815–824. [PubMed: 16039535]
57. Fei B, Kemper C, Wilson DL. A comparative study of warping and rigid body registration for the prostate and pelvic MR volumes. Comput Med Imaging Graph 2003;27:267–281. [PubMed: 12631511]

58. Venugopal N, McCurdy B, Hnatov A, Dubey A. A feasibility study to investigate the use of thin-plate splines to account for prostate deformation. Phys Med Biol 2005;50:2871–2885. [PubMed: 15930608]
59. Fei B, Duerk JL, Wilson DL. Automatic 3D registration for interventional MRI-guided treatment of prostate cancer. Comput Aided Surg 2002;7:257–267. [PubMed: 12582978]
60. Fei B, Wheaton A, Lee Z, Duerk JL, Wilson DL. Automatic MR volume registration and its evaluation for the pelvis and prostate. Phys Med Biol 2002;47:823–838. [PubMed: 11931473]
61. Wu X, Dibiase SJ, Gullapalli R, Yu CX. Deformable image registration for the use of magnetic resonance spectroscopy in prostate treatment planning. Int J Radiat Oncol Biol Phys 2004;58:1577–1583. [PubMed: 15050339]
62. Lee Z, Nagano KK, Duerk JL, Sodee DB, Wilson DL. Automatic registration of MR and SPECT images for treatment planning in prostate cancer. Acad Radiol 2003;10:673–684. [PubMed: 12809423]
63. Pasquier D, Lacornerie T, Vermandel M, Rousseau J, Lartigau E, Betrouni N. Automatic segmentation of pelvic structures from magnetic resonance images for prostate cancer radiotherapy. Int J Radiat Oncol Biol Phys 2007;68:592–600. [PubMed: 17498571]
64. Tsai A, Wells W, Tempany C, Grimson E, Willsky A. Coupled multi-shape model and mutual information for medical image segmentation. Inf Process Med Imaging 2003;18:185–197. [PubMed: 15344457]
65. Barnes AS, Haker SJ, Mulkern RV, So M, D'Amico AV, Tempany CM. Magnetic resonance spectroscopy-guided transperineal prostate biopsy and brachytherapy for recurrent prostate cancer. Urology 2005;66:1319. [PubMed: 16360468]
66. Chan I, Wells W 3rd, Mulkern RV, et al. Detection of prostate cancer by integration of line-scan diffusion, T2-mapping and T2-weighted magnetic resonance imaging; a multichannel statistical classifier. Med Phys 2003;30:2390–2398. [PubMed: 14528961]
67. Selli C, Caramella D, Giusti S, et al. Value of image fusion in the staging of prostatic carcinoma. Radiol Med (Torino) 2007;112:74–81. [PubMed: 17310289]
68. Lee JS, Chung BH. Transrectal ultrasound versus magnetic resonance imaging in the estimation of prostate volume as compared with radical prostatectomy specimens. Urol Int 2007;78:323–327. [PubMed: 17495490]
69. Rahmouni A, Yang A, Tempany CM, et al. Accuracy of in-vivo assessment of prostatic volume by MRI and transrectal ultrasonography. J Comput Assist Tomogr 1992;16:935–940. [PubMed: 1385499]
70. Smith WL, Lewis C, Bauman G, et al. Prostate volume contouring: a 3D analysis of segmentation using 3DTRUS, CT, and MR. Int J Radiat Oncol Biol Phys 2007;67:1238–1247. [PubMed: 17336224]
71. Schreibmann E, Xing L. Narrow band deformable registration of prostate magnetic resonance imaging, magnetic resonance spectroscopic imaging, and computed tomography studies. Int J Radiat Oncol Biol Phys 2005;62:595–605. [PubMed: 15890605]
72. Mizowaki T, Cohen GN, Fung AY, Zaider M. Towards integrating functional imaging in the treatment of prostate cancer with radiation: the registration of the MR spectroscopy imaging to ultrasound/CT images and its implementation in treatment planning. Int J Radiat Oncol Biol Phys 2002;54:1558–1564. [PubMed: 12459385]
73. Lattouf JB, Grubb RL 3rd, Lee SJ, et al. Magnetic resonance imaging-directed transrectal ultrasonography-guided biopsies in patients at risk of prostate cancer. BJU Int 2007;99:1041–1046. [PubMed: 17437438]
74. Daanen V, Gastaldo J, Giraud JY, et al. MRI/TRUS data fusion for brachytherapy. Int J Med Robot 2006;2:256–261. [PubMed: 17520640]
75. Reynier C, Troccaz J, Fourneret P, et al. MRI/TRUS data fusion for prostate brachytherapy. Preliminary results Med Phys 2004;31:1568–1575.
76. Gelet A, Chapelon JY, Bouvier R, Pangaud C, Lasne Y. Local control of prostate cancer by transrectal high intensity focused ultrasound therapy: preliminary results. J Urol 1999;161:156–162. [PubMed: 10037389]

77. Gelet A, Chapelon JY, Bouvier R, Rouviere O, Lyonnet D, Dubernard JM. Transrectal high intensity focused ultrasound for the treatment of localized prostate cancer: factors influencing the outcome. Eur Urol 2001;40:124–129. [PubMed: 11528187]

78. McDannold N, King RL, Jolesz FA, Hynynen K. The use of quantitative temperature images to predict the optimal power for focused ultrasound surgery: in vivo verification in rabbit muscle and brain. Med Phys 2002;29:356–365. [PubMed: 11929019]

79. Hynynen K, Pomeroy O, Smith DN, et al. MR imaging-guided focused ultrasound surgery of fibroadenomas in the breast: a feasibility study. Radiology 2001;219:176–185. [PubMed: 11274554]

80. Tempany CM, Stewart EA, McDannold N, Quade BJ, Jolesz FA, Hynynen K. MR imaging-guided focused ultrasound surgery of uterine leiomyomas: a feasibility study. Radiology 2003;226:897–905. [PubMed: 12616023]

81. Fischer, GS.; DiMaio, SP.; Iordachita, I.; Fichtinger, G. Development of a robotic assistant for needle-based transperineal prostate interventions in MRI. Proc 10th Int'l Conference on Medical Image Computing and Computer-Assisted Intervention; MICCAI 2007. Nov. 2007; p. 425-433.LNCS 4791

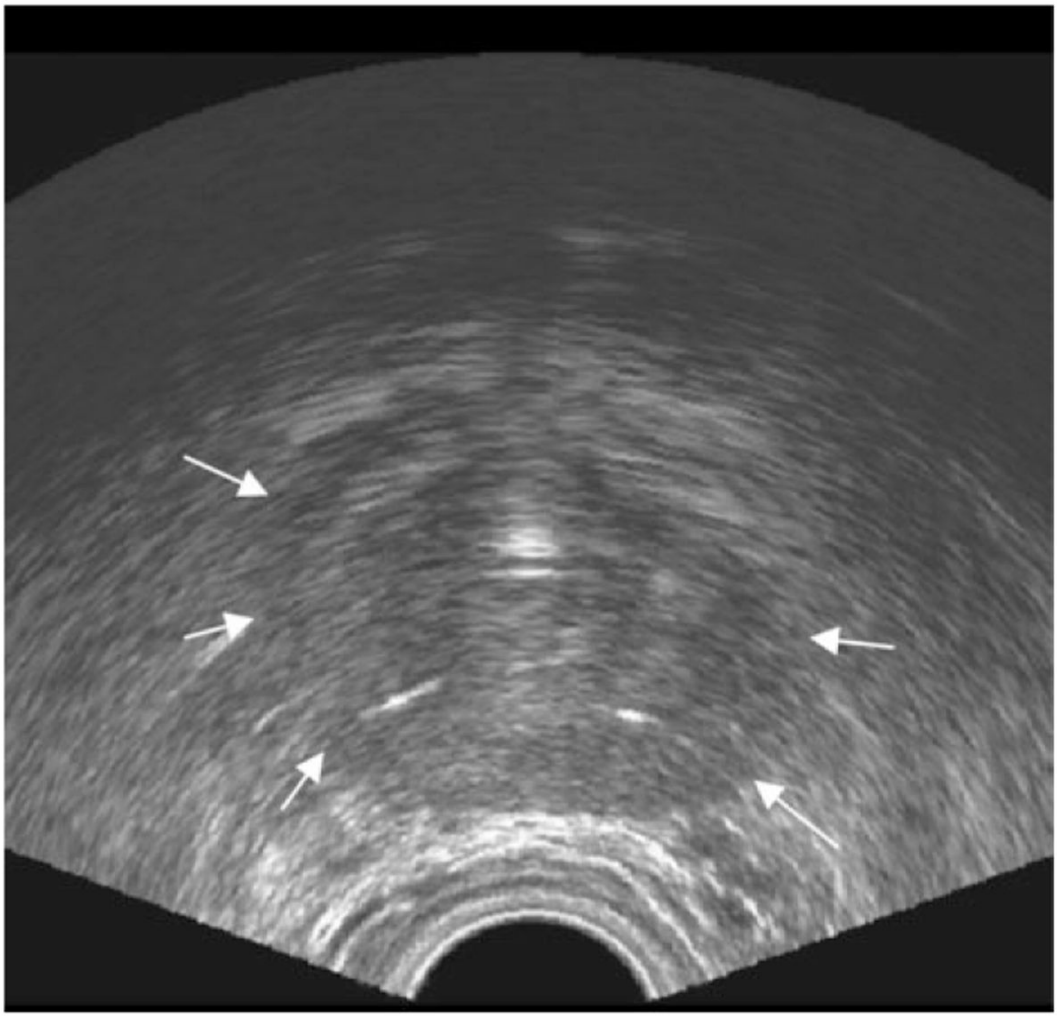

Figure 1.
Prostate ultrasound. Axial transrectal ultrasound image of the prostate. Arrows indicate prostate capsule boundary.

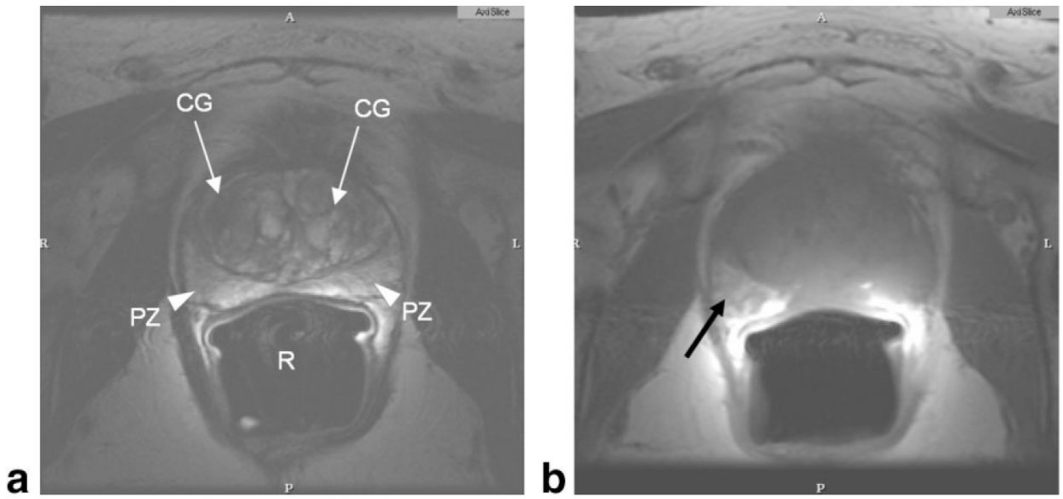

Figure 2.

Normal prostate MRI. Axial T2W (**a**), and axial T1W (**b**) image of prostate taken at 1.5T using an endorectal coil. Central gland (CG, white arrows) in the T2W image shows benign prostate hyperplasia. Peripheral zone is indicated as PZ (white arrowheads). Air in the rectum (R) is due to the endorectal coil balloon. Hyperintense region of the right peripheral zone in the T1-weighted image (black arrow) indicates hemorrhage.

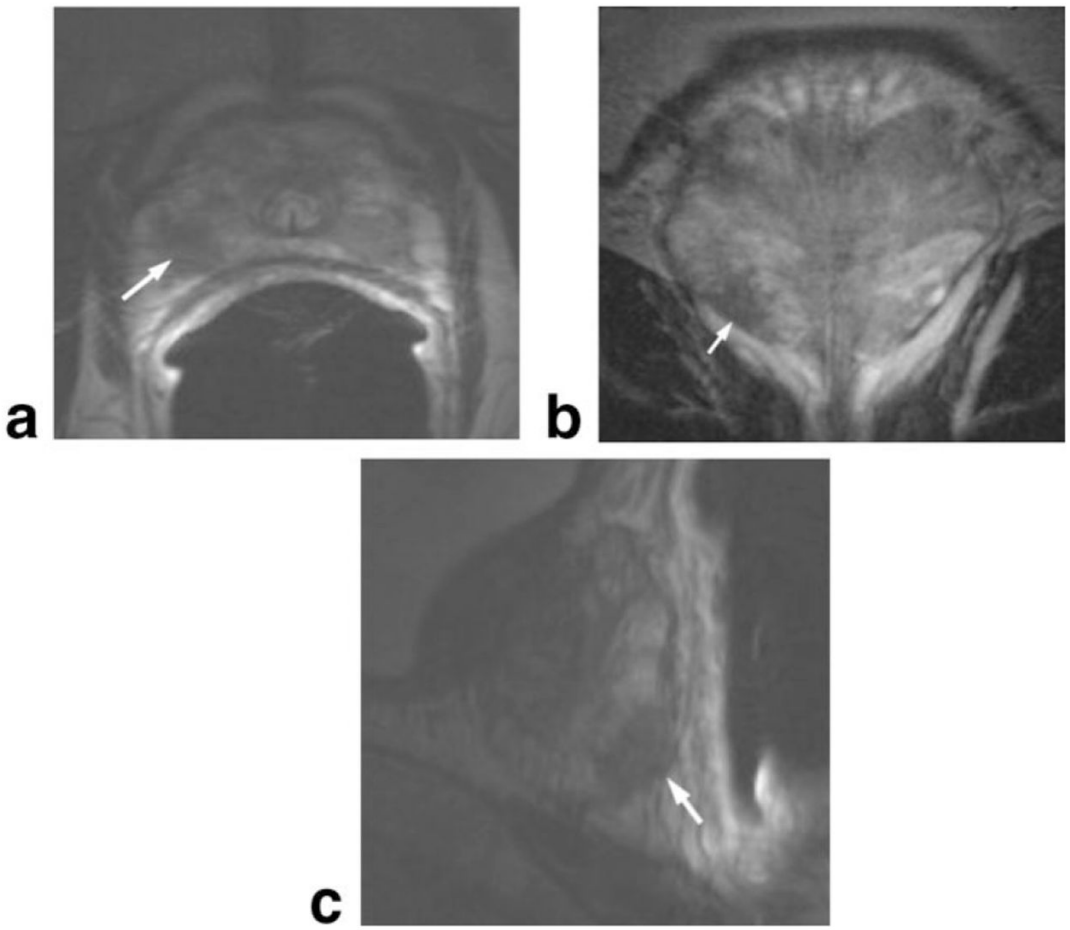

Figure 3.
Multiplanar prostate MR. Axial (**a**), coronal (**b**), and sagittal (**c**) T2W prostate images taken at 1.5T using an endorectal coil in a patient with prostate cancer. Tumor in right apical region of the gland (arrows), indicated by low signal, can be seen in all three planes.

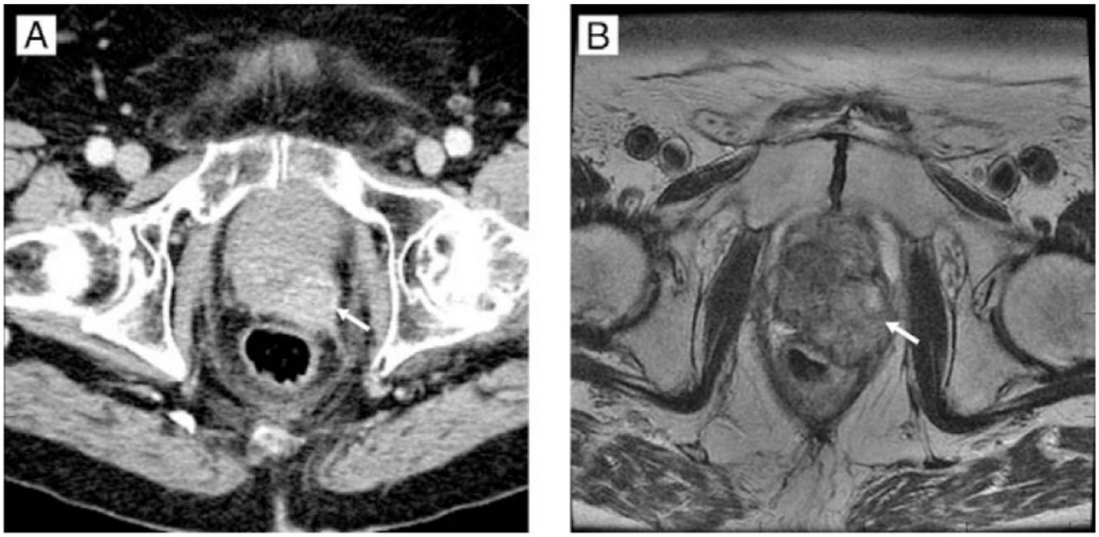

Figure 4.
Advanced prostate cancer. Prostate CT and corresponding MR. **a:** CT image of the prostate using early-phase intravenous contrast. **b:** Corresponding axial T2W MR at 1.5T, obtained using a body coil but no endorectal coil. White arrows indicate a focal tumor in the left posterior region of the prostate.

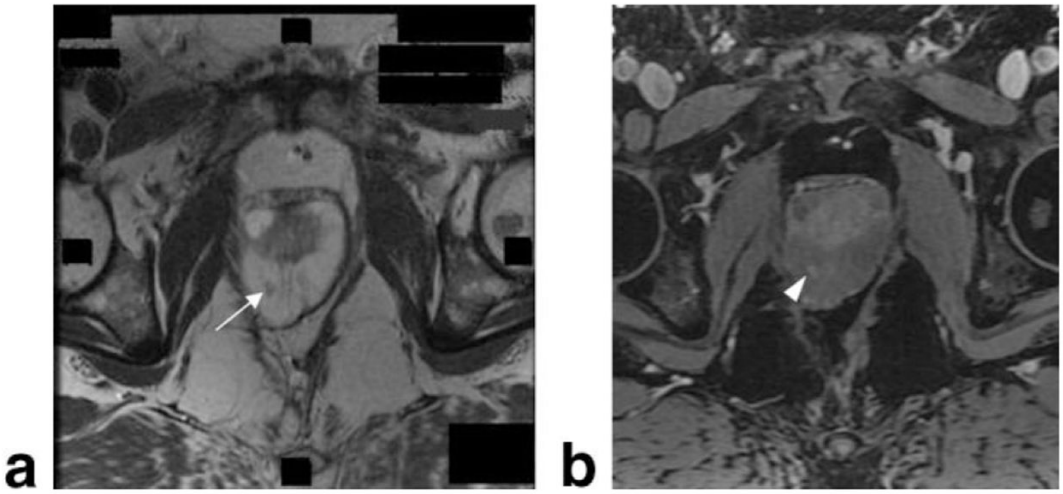

Figure 5.
MR of the prostate at 3T. Axial MRI of the prostate obtained prior to biopsy at 3T using a body coil. Prior rectal surgery precluded the use of an endorectal coil. Within T2W image (**a**), low signal region (white arrow) indicates a focal lesion in the right mid-gland. T1-weighted image (**b**) shows postgadolinium contrast enhancement of the lesion (white arrowhead).

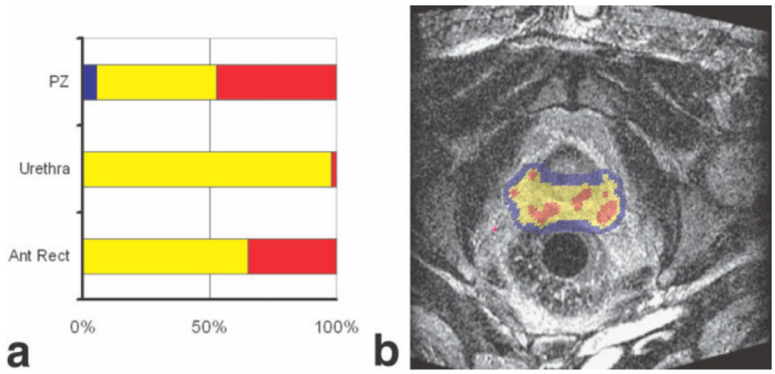

Figure 6.

MR-based brachytherapy planning. A screen capture of a treatment planning system used for MR-guided brachytherapy is shown. The large image (**b**) shows a real-time image with levels of radiation dose indicated by a color wash. Colors are used to indicate the relation between delivered dose and either the dose prescribed to the target or dose limits of the surrounding normal structures. Each structure is assigned a structure specific minimum and maximum dose. Dose summary graphs (**a**) show the fraction of each structure receiving below minimum (blue), between minimum and maximum (yellow), and over maximum (red). Normal structures will have a minimum dose of 0 and a maximum dose related to their tolerance of radiation. Target structures will have minimum dose that is the prescription dose and a maximum dose taken as 150% of the prescription. Due to the nature of brachytherapy, any target will have significant regions above the structure's maximum dose. The regions of interest are delineated on a reference set of images taken at the beginning of the procedure. Dose is calculated based on needle locations as observed on images acquired during the course of the implant procedure. The planning system enables adaptive treatment planning.

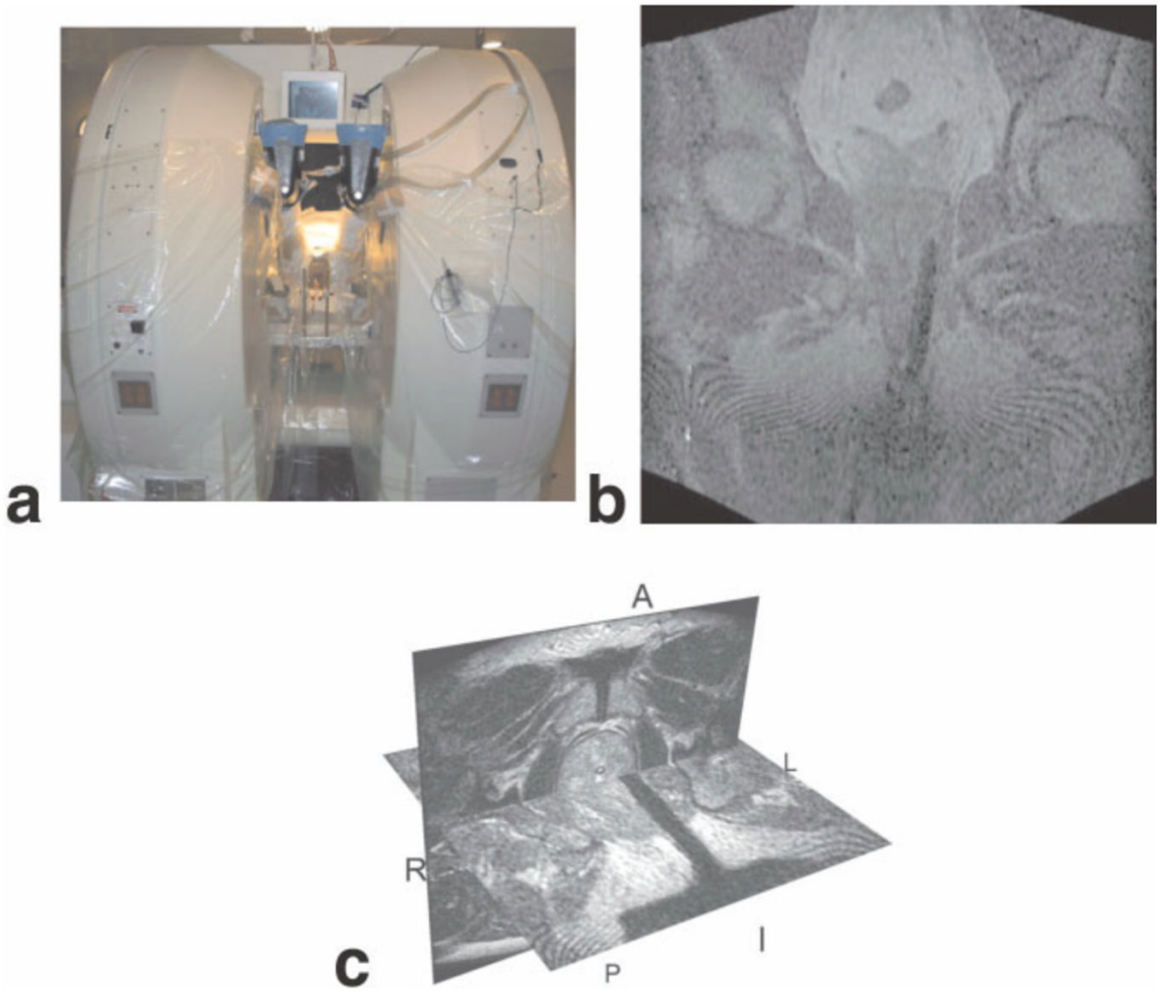

Figure 7.
MR-guided prostate biopsy. The MRT Signa/SP system (**a**) setup for MRI-guided prostate biopsy. Coronal FGR image (**b**) showing biopsy needle inserted on the left side. 3D Slicer (**c**) showing the combination of the needle on FGR image with the T2-weighted image of the prostate.

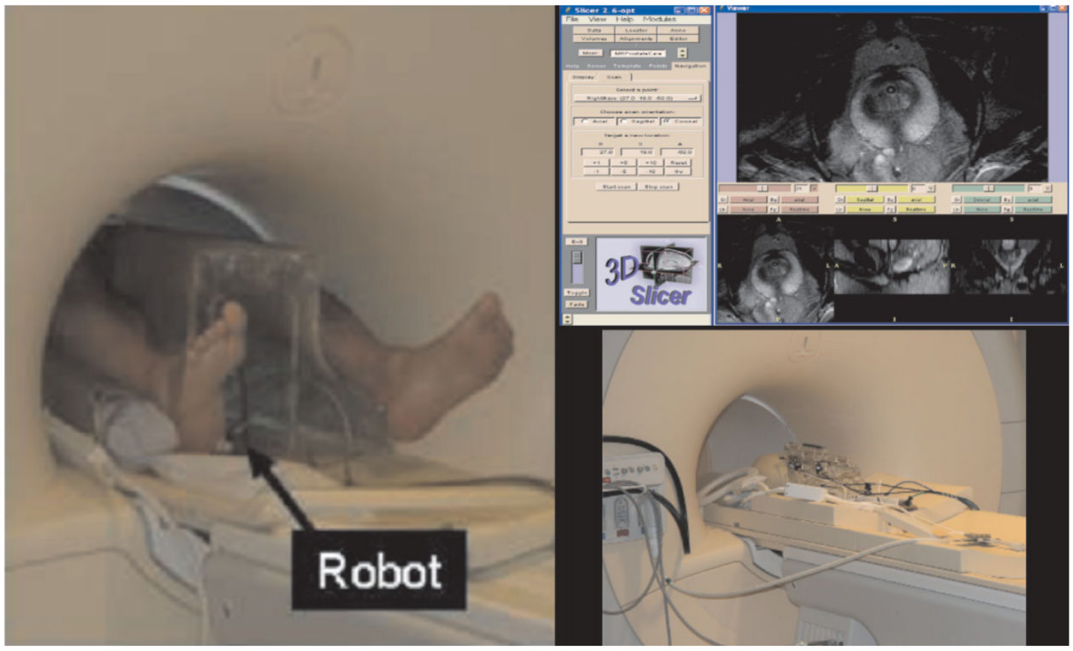

Figure 8.

At top right, the 3D Slicer software platform used for MRI-guided biopsy. The 3D Slicer provides guidance and navigation during MRI-guided biopsy, allowing for multiplanar views of image volumes, target selection, and control of the MR scanner imaging plane. Here, T2W images obtained in the axial plane are shown. The control panel shown is used for slice selection to ensure that the real-time planar imaging obtained during needle insertion contains the desired target. On the left, a robotic assistant system for prostate intervention in a 3T closed-bore MRI scanner. The robot is placed between the patient's legs and the MRI compatible mechanism (bottom right). The pneumatic actuator ensures no interference to MR images.

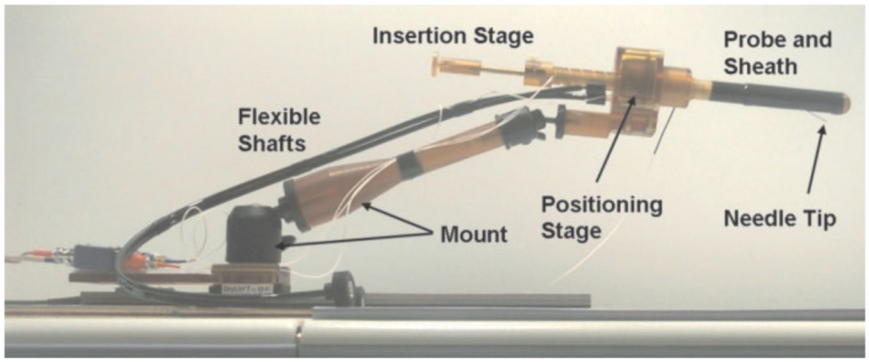

Figure 9.
Johns Hopkins prostate biopsy manipulator. Picture of the Johns Hopkins manipulator for prostate biopsy and gold marker placements showing the different components and the needle tip, showing needle guide and sheath, positioning stage, flexible actuation shafts, and mount. Reproduced with permission, ©2005 IEEE. Courtesy of A. Krieger.

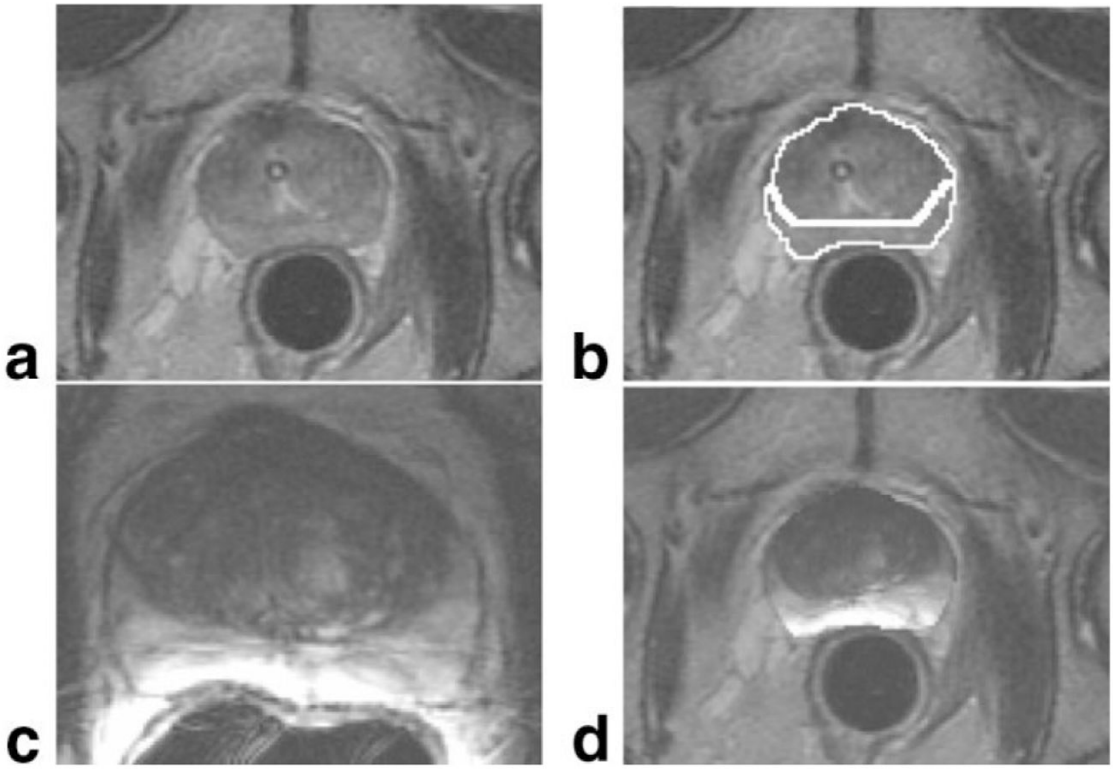

Figure 10.

An example of MR to MR finite element based registration for brachytherapy treatment planning. Intraoperative axial T2-weighted imaging at 0.5T of the prostate (**a**) is manually contoured (**b**) to delineate the glandular boundary. The prostate gland, as seen in preoperative 1.5T T2W axial image obtained with an endorectal coil (**c**). This is registered to the contoured capsule to produce an integrated view of preoperative imaging within the intraoperative imaging space (**d**). The registration process here is done in three dimensions; all intraoperative images containing the prostate are manually contoured as a normal part of MRI-guided brachytherapy treatment planning. Note the significant shape change that occurs. This is due to a difference in leg position and the use of an endorectal coil during the preoperative scan.

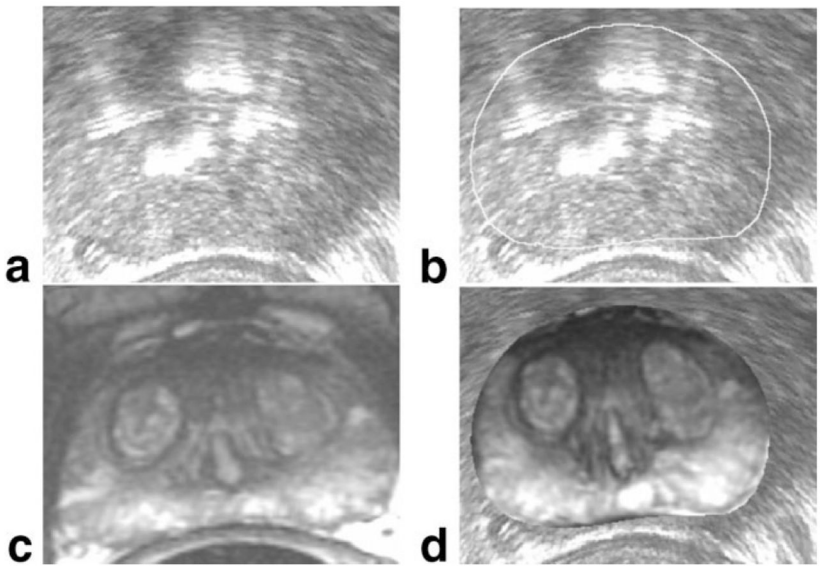

Figure 11.
MR to ultrasound registration for brachytherapy treatment planning. Similar to the case shown in Fig. 10, intraoperative axial ultrasound imaging of the prostate (**a**) is manually contoured (**b**) to delineate the glandular boundary. Preoperative 1.5T T2-weighted axial MR imaging (**c**), obtained with an endorectal coil, is registered to the contoured capsule to produce an integrated view of preoperative imaging within the intraoperative imaging space (**d**).